J Appl Electrochem (2016) 46:85–101
DOI 10.1007/s10800-015-0901-5

RESEARCH ARTICLE

Numerical investigation of combined chemical and electrochemical processes in Fe_2O_3 suspension electrolysis

V. A. Danilov[1]

Received: 30 May 2015 / Accepted: 26 October 2015 / Published online: 13 November 2015

Abstract Suspension electrolysis is a combined process of chemical and electrochemical reactions. The developed model for a parallel-plate electrochemical reactor is based on mixture model for suspension flow and balance equation for diluted species taking into account the dispersed phase content and ions migration due to the electrolyte current and partial dissolution of suspended particles in the suspension electrolysis. Electrochemical reactions are specified through flux boundary conditions at the electrode/electrolyte interface. The influence of the combined processes is reflected through the distribution of ions concentration profile in liquid phase and current density profile at the electrode surface. Numerical investigation indicates that about 90 % of the iron deposition flux is accommodated by an additional component flux due to the chemical reaction of partial dissolution of α-Fe_2O_3 particles in suspension electrolysis.

Keywords Suspension electrolysis · Parallel-plate reactor · Combined processes · Deposition · Dissolution

List of symbols

a	Activity (mol l^{-1})
a_v	Interfacial area (m^2 m^{-3})
c	Molar concentration (mol m^{-3})
C_{dl}	Double layer capacitance (F m^{-2})
d_p	Diameter of particle (m)
D	Diffusion coefficient (m^2 s^{-1})
D_a	Dispersion coefficient (m^2 s^{-1})
E_{cell}	Cell voltage (V)
E_0	Reversible potential (V)
F	Faraday's constant (96,485 C mol^{-1})
k	Conductivity (Ω^{-1} m^{-1})
I	Current density (A m^{-2})
I_0	Exchange current density (A m^{-2})
N	Molar flow (mol s^{-1})
n_e	Number of electrons
P	Pressure (Pa)
R	Ideal gas constant (J mol^{-1} K^{-1})
R^{cell}	Ohmic resistance (Ω m^2)
r	Source term (mol m^{-3} s^{-1})
S	Electrode area (m^2)
T	Temperature (K)
$\mathbf{u}$	Velocity vector (m s^{-1})
V	Volume (m^3)
x	OX co-ordinate
y	OY co-ordinate
z	OZ co-ordinate

Greek letters

α	Dissociation constant
α_A	Anodic charge transfer coefficients
α_C	Cathodic charge transfer coefficients
α_G	Volume fraction of gas phase (m^3 m^{-3})
β_f	Mass transfer coefficient (m s^{-1})
ε_d	Suspension volume fraction (m^3 m^{-3})
Γ	Source term (kg m^{-3} s^{-1})
ν	Stoichiometry coefficient
η	Potential difference (V)
ρ	Density (kg m^{-3})
δ_E	Distance between electrodes (m)
τ	Time (s)
φ	Potential (V)

✉ V. A. Danilov
danilov.valery.antipovich@gmail.com

[1] School of Engineering, Far Eastern Federal University, Ajax Bay, Russky Island, Vladivostok, Russia 690922

Subscripts/superscripts

A	Anode electrode
avg	Averaged
c	Continuous
C	Cathode electrode
cell	Electrochemical reactor
d	Dispersed
e	Electrolyte
eff	Effective
eq	Equilibrium
in	Inlet
L	Liquid
mol	Molar
ref	Reference

1 Introduction

Combined processes are widely used in chemical and electrochemical industry. Suspension electrolysis is an example of the combined chemical and electrochemical processes in an electrochemical reactor. Experimental data on suspension electrolysis are available in literature for different systems [1–6]. Okada et al. [1] studied the electrolysis of coal under potentiostatic conditions using suspended coals in sulfuric acid solution. Fourcade and Tzedakis [2] studied the kinetics of silver electrodeposition from a suspension of silver iodide in aqueous media using a rotating disk electrode. Paramguru et al. [3] examined electrochemical extraction of lead from galena by suspension electrolysis using galvanostatic and voltammetric studies in various electrolytes. Allanore et al. [4–6] investigated the feasibility of iron production by electrolysis of hematite particles suspension in a strong alkaline medium. They used three electrolysis configurations using 13 % suspension with particle size distribution of hematite particles ranging from 0.4 to 10 μm. Their results stress that the low-temperature electrolysis technology is a potential method to produce steel with very low CO_2 emission.

Electrochemical processes in multiphase flow requires further investigation. Modeling is important for understanding the mechanism of combined processes and improving the electrochemical reactor performance. Numerical simulation is able to identify the main transfer processes governing the suspension electrolysis. The primary goal of this study is to develop a model of transfer processes in a parallel-plate reactor for numerical investigation of iron deposition taking into account the combined chemical and electrochemical processes in suspension electrolysis.

2 Model development

Wang and Gu [7, 8] developed a micro-macroscopic coupled model for advanced batteries and electrochemical cells with multiphase system using the volume averaging technique. For multiphase transfer processes in an electrochemical reactor, macroscopic conservation equations are defined for liquid phase using the volume averaging technique taking into account interfacial momentum and mass transfer. Application of macroscopic conservation equations for electrochemical processes with porous electrode is shown in literature [9, 10]. For multiphase electrochemical processes in suspension electrolysis, the description of transfer processes is based on macroscopic conservation equations proposed by Wang and Gu [7, 8].

Suspension electrolysis is performed in a parallel-plate reactor operating under galvanostatic mode. Suspension at the inlet section is two-phase flow of continuous 50 % NaOH solution with 10 μm α-Fe_2O_3 particles. The following assumptions are used in the model development: (i) isothermal two-phase flow is homogeneous without interaction between particles; (ii) electrochemical reactions occur at the electrode/electrolyte interface; (iii) flow is symmetric in the Ox direction; (iv) concentration of ions is in equilibrium with the dispersed solid phase at the inlet section; (v) the effect of gas content on physical properties and conductivity is negligible. The assumption of mixture model is that velocity of the dispersed phase is equal to the velocity of continuous liquid phase due to the uniform distribution of the suspended solid particles in a local volume.

A CFD model of parallel-plate electrochemical reactor in suspension electrolysis is developed using COMSOL Multiphysics, the Mixture model Module, the Transport of diluted species Module, and the Boundary ODE Module. Assuming that flow is symmetrical with respect to the longitudinal axis, the CFD model considers the half part of the parallel-plate reactor. For suspension electrolysis in a parallel-plate electrochemical reactor, the governing equations are given in Table 1.

The velocity profile in the reactor is described by homogeneous mixture model. The concentration profile in continuous liquid phase is defined by conservation equation for diluted species taking into account volume fraction of the dispersed phase together with diffusion and migration processes. Dispersion coefficient takes into account an additional component flux in the diluted species conservation equation due to the variation of velocity near the particles in two-phase flow. Potential profile in the electrolyte is governed by charge balance equation. Electrochemical reactions are specified through the boundary condition at the corresponding electrode/electrolyte interface. For cathode

Table 1 Definition of balance equations for parallel-plate reactor

Balance equation	Expression
Mixture model, laminar flow	$\rho\frac{\partial \mathbf{u}}{\partial t}+\rho(\mathbf{u}\cdot\nabla)\mathbf{u}=\nabla\cdot\left[-p\mathbf{I}+\mu\left(\nabla\mathbf{u}+(\nabla\mathbf{u})^{T}\right)\right]+\rho\mathbf{g}$
	$\rho_{\mathrm{c}}(\nabla\cdot\mathbf{u})=\Gamma_{\mathrm{d}}(\rho_{\mathrm{d}}-\rho_{\mathrm{c}})/\rho_{\mathrm{c}}$
	$\frac{\partial \varepsilon_{\mathrm{d}}}{\partial t}+\nabla\cdot(\varepsilon_{\mathrm{d}}\mathbf{u})=-\Gamma_{\mathrm{d}}/\rho_{\mathrm{d}},\ \rho=\rho_{\mathrm{c}}(1-\varepsilon_{\mathrm{d}})+\rho_{\mathrm{d}}\varepsilon_{\mathrm{d}},\ \mathbf{u}_{\mathrm{slip}}=0$
Transport of diluted species with convection and migration, Nernst–Planck equations	$\frac{\partial \varepsilon_{\mathrm{L}}c^{(i)}}{\partial t}+\nabla\cdot\mathbf{N}^{(i)}+\mathbf{u}\cdot\nabla\left(\varepsilon_{\mathrm{L}}c^{(i)}\right)=r^{(i)},\ i=\ \mathrm{Fe(OH)_4^-},\ \mathrm{OH^-},\ \mathrm{H^+}$
	$\mathbf{N}^{(i)}=-\left(D_{\mathrm{eff}}^{(i)}+D_{\mathrm{a}}^{(i)}\right)\nabla c^{(i)}-z^{(i)}u_{\mathrm{m,eff}}^{(i)}\mathrm{F}c^{(i)}\nabla\varphi$
	$r^{\mathrm{Fe(OH)_4^-}}=\Gamma_{\mathrm{d}}/M^{\mathrm{Fe(OH)_4^-}},\ r^{\mathrm{OH^-}}=0,\ r^{\mathrm{Na^+}}=0,\ \varepsilon_{\mathrm{L}}=1-\varepsilon_{\mathrm{d}},\ D_{\mathrm{a}}^{(i)}=0$
Transport of diluted species	$\frac{\partial \varepsilon_{\mathrm{L}}c^{(i)}}{\partial t}+\nabla\cdot\mathbf{N}^{(i)}+\mathbf{u}\cdot\nabla\left(\varepsilon_{\mathrm{L}}c^{(i)}\right)=0,\ i=\ \mathrm{O_2},\ \mathrm{H_2}$
	$\mathbf{N}^{(i)}=-\left(D_{\mathrm{eff}}^{(i)}+D_{\mathrm{a}}^{(i)}\right)\nabla c^{(i)},\ D_{\mathrm{a}}^{(i)}=0$
Primary current distribution, electrolyte suspension	$k_{\mathrm{s}}\cdot\nabla\varphi=0$

electrochemical reaction of hydrogen evolution, distribution of the dissolved hydrogen in liquid phase is described by conservation equation for diluted species taking into account volume fraction of the dispersed solid phase. For anode electrochemical reaction of oxygen evolution, distribution of dissolved oxygen in liquid phase is described by the diluted species conservation equation taking into account volume fraction of the dispersed solid phase.

2.1 Boundary conditions

The boundary condition for liquid electrolyte inlet has a prescribed uniform velocity and species concentrations (Table 2). Homogeneous suspension with uniform inlet velocity, species concentration, and solid phase volume fraction is fed at the inlet section of parallel-plate electrochemical reactor as shown in Fig. 1. Continuous liquid phase of NaOH electrolyte contains Fe^{+3}, OH^-, Na^+, and H^+ ions. Taking into account experimental data [11] on Fe(III) hydrolysis and ions stability, it is concluded that $Fe(OH)_4^-$ ions predominate in alkaline media. The inlet concentration of $Fe(OH)_4^-$ ions is set equal to the equilibrium concentration of partial dissolution of α-Fe_2O_3 solid particles in alkaline (NaOH) solution. The inlet concentration of OH^- and Na^+ ions is calculated using the dissociation constant of NaOH electrolyte. Anode electrochemical reaction is defined as flux boundary condition at the anode electrode/electrolyte interface. Cathode electrochemical reaction is defined as flux boundary condition for species at the cathode electrode/electrolyte interface (Table 2). Stoichiometric coefficients are given by overall cathode and anode electrochemical reactions [4–6].

For charge balance at the electrode/electrolyte interface, the source term on the right side is a difference of electrode and electrolyte (cell) current densities normal to the boundary as shown in Appendix 1. For a parallel-plate electrochemical reactor operating under galvanostatic mode ($I_{\mathrm{cell}}=\mathrm{const}$), the cell current density is specified as electrolyte current density at the electrode/electrolyte interface. The total current density at the cathode electrode is a sum of partial current densities corresponding to the iron deposition and hydrogen evolution electrochemical reactions at the cathode electrode/electrolyte interface. Hydrogen dissolved in the liquid phase participates in the electrochemical reaction of hydrogen oxidation at the

Table 2 Boundary conditions for parallel-plate reactor

Section	Expression
Inlet section $x=0$	$u=u_{\mathrm{in}},\ \varepsilon_{\mathrm{d}}=\varepsilon_{\mathrm{d,in}},\ \partial\varphi/\partial x=0$
	$c=c_{\mathrm{in}}^{(k)},\ k=\ \mathrm{Fe(OH)_4^-},\ \mathrm{OH^-},\ \mathrm{Na^+}$
Outlet section $x=L$	$p=0,\ \partial u/\partial x=0,\ \partial\varphi/\partial x=0,\ \partial\varepsilon_{\mathrm{d}}/\partial y=0$
	$\partial c^{(k)}/\partial x=0,\ k=\ \mathrm{Fe(OH)_4^-},\ \mathrm{OH^-},\ \mathrm{Na^+}$
Symmetry $y=B$	$\partial u/\partial y=0,\ \partial\varepsilon_{\mathrm{d}}/\partial y=0,\ \partial\varphi/\partial x=0$
	$\partial c^{(k)}/\partial y=0,\ k=\ \mathrm{Fe(OH)_4^-},\ \mathrm{OH^-},\ \mathrm{Na^+}$
Anode electrode $z=h$	$-\mathbf{n}\cdot\mathbf{N}^{(k)}=\frac{\nu^{(k)}}{n_e^{(k)}F}I^{\mathrm{A}},\ k=\ \mathrm{OH^-},\ \mathrm{O_2}$
	$C_{\mathrm{dl}}\frac{\partial\eta^{\mathrm{A}}}{\partial t}=-\nabla\cdot I_{\mathrm{s}}+(I^{\mathrm{A}}-I_e)$
	$\varphi=V_{\mathrm{cell}}-\eta^{\mathrm{A}}$
	$\partial\varepsilon_{\mathrm{d}}/\partial y=0$
Cathode electrode $z=0$	$-\mathbf{n}\cdot\mathbf{N}^{(k)}=\frac{\nu^{(k)}}{n_e^{(k)}F}\lvert I^{\mathrm{C}}\rvert,\ k=\ \mathrm{Fe(OH)_4^-}$
	$-\mathbf{n}\cdot\mathbf{N}^{(k)}=\frac{\nu^{(k)}}{n_e^{(k)}F}\lvert I_{\mathrm{H_2}}\rvert,\ k=\ \mathrm{OH^-},\ \mathrm{H_2}$
	$C_{\mathrm{dl}}\frac{\partial\eta^{\mathrm{C}}}{\partial t}=-\nabla\cdot I_{\mathrm{s}}-((I^{\mathrm{C}}+I^{\mathrm{H_2}})-I_e)$
	$\varphi=0-\eta^{\mathrm{C}}$
	$c_{\mathrm{H^+}}=c_{\mathrm{eq}}^{\mathrm{H^+}},\ \varepsilon_{\mathrm{d}}=0.62$

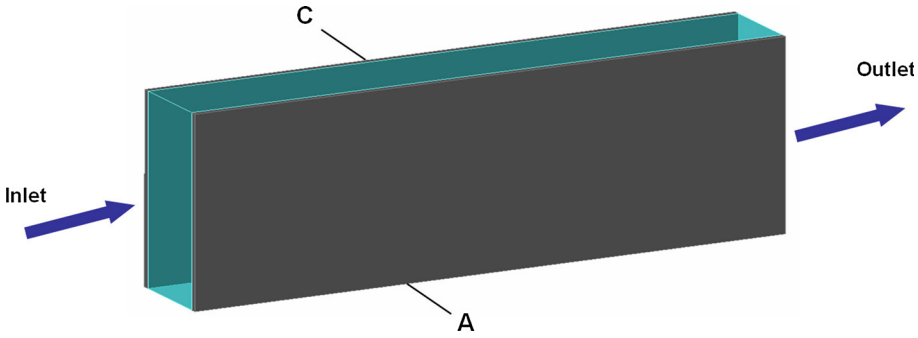

Fig. 1 Parallel-plate reactor for suspension electrolysis. *C* Cathode electrode, *A* anode electrode

cathode electrode. Assuming that electrochemical reaction of hydrogen oxidation is at equilibrium, concentration of hydrogen ions H^+ at the cathode electrode surface is set equal to the equilibrium concentration calculated from the corresponding Nernst equation (Appendix 2).

Allanore et al. [12] proposed a quantitative method for analysis of the particle-electrode interaction in the suspension electrolysis. They observed the film of adsorbed particles on the cathode steel surface in the sodium hydroxide electrolyte during the experiments. Taking into account experimental data [12], volume fraction of the dispersed phase at the cathode boundary is set equal to the maximum packing fraction of particles ($\varepsilon_d = 0.62$).

2.2 Numerical procedure

The developed model was implemented in COMSOL Multiphysics using generic transport equations given in Table 1. The computational domain of parallel-plate reactor is shown in Fig. 2. Three mesh designs (case I, case II, and case III) are compared in terms of computed pressure and velocity to ensure a mesh independent solution. The boundary layer is specified using a special boundary mesh with 10^{-8} step size on anode and cathode side. The results show that solution with mesh in case II (87,254 elements) differs only about 3 % in terms of pressure and velocity with a finer mesh in case III (107,281 elements). Mesh with case I (15,793 elements) gives a deviation of 25 % compared to the finest mesh. Hence, the mesh with case II was used to obtain solution with reasonable computational time.

3 The electrochemistry

3.1 Anode electrochemical reactions

During suspension electrolysis, OH^- ions are consumed at the anode electrode/electrolyte interface and produced at the cathode electrode/electrolyte interface. The transport of diluted species is defined taking into account convection, diffusion, and migration mechanisms in the liquid electrolyte together with the volume fraction of the dispersed phase (Table 1). The overall anode electrochemical reaction of oxygen evolution in alkaline media is

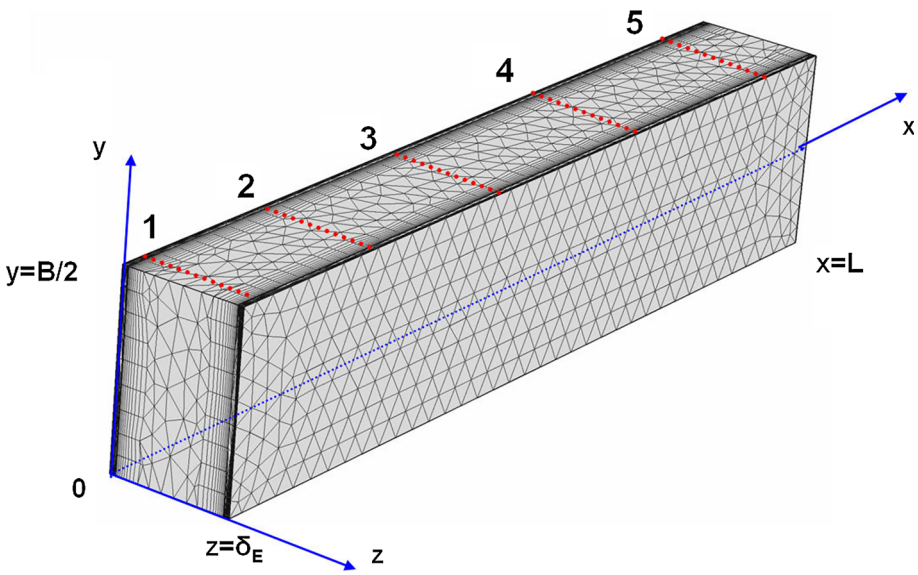

Fig. 2 Computational domain of parallel-plate reactor. *L* electrode length, *B* electrode width, δ_E distance between anode and cathode electrodes, *1* plane $x = 0.0017$ m intersecting plane $y = B/2$, *2* plane $x = 0.017$ m intersecting plane $y = B/2$, *3* plane $x = 0.034$ m intersecting plane $y = B/2$, *4* plane $x = 0.051$ m intersecting plane $y = B/2$, *5* plane $x = 0.068$ m intersecting plane $y = B/2$

$$4OH^- \rightarrow O_2 + 2H_2O + 4e^- \quad \left(E^0 = 0.4 \text{ V vs. SHE}\right) \tag{1}$$

Taking into account the mechanism of oxygen evolution [13, 14], the rate of electrochemical reaction (1) is written as follows:

$$I^{\mathrm{A}} = I_0^{\mathrm{A}} \left(\frac{c_{\mathrm{A}}^{\mathrm{OH}^-}}{c_{\mathrm{ref}}^{\mathrm{OH}^-}}\right) \left(\exp\left(\frac{\alpha_{\mathrm{A}}^{\mathrm{A}} F}{\mathrm{RT}}\left(\eta^{\mathrm{A}} - \eta_{\mathrm{eq}}^{\mathrm{A}}\right)\right) - \exp\left(-\frac{\alpha_{\mathrm{C}}^{\mathrm{A}} F}{\mathrm{RT}}\left(\eta^{\mathrm{A}} - \eta_{\mathrm{eq}}^{\mathrm{A}}\right)\right)\right), \tag{2}$$

where I_0^{A} is the anode exchange current density; $c_{\mathrm{ref}}^{\mathrm{OH}^-}$ is the reference concentration for OH^- ions; η^{A} is the potential difference at the anode electrode/electrolyte interface. The equilibrium potential for reaction (1) is

$$\eta_{\mathrm{eq}}^{\mathrm{A}} = E_0^{\mathrm{A}} - \frac{\mathrm{RT}}{n_e^{\mathrm{A}} F} \ln\left(\left(a_{\mathrm{A}}^{\mathrm{OH}^-}\right)^4\right). \tag{3}$$

3.2 Cathode electrochemical reactions

The mechanism of cathodic iron deposition in alkaline media is given by Hurlen [15]

$$Fe^{+3} + e^- \rightarrow Fe^{+2} \quad \text{Equilibrium} \tag{4}$$

$$2Fe^{+2} + 4e^- \rightarrow 2Fe \quad \text{rds} \ \left(E_0^{\mathrm{C}} = -0.467 \text{ V}\right) \tag{5}$$

The rate of iron deposition is [15]

$$I_{\mathrm{C}}^{\mathrm{Fe}} = I_0^{\mathrm{Fe}} \left(\frac{c^{\mathrm{Fe}^{+2}}}{c_{\mathrm{ref}}^{\mathrm{Fe}^{+2}}}\right)^2 \left(\frac{c^{\mathrm{OH}^-}}{c_{\mathrm{ref}}^{\mathrm{OH}^-}}\right) \left(\exp\left(\frac{\alpha_{\mathrm{A}}^{\mathrm{C}} F}{\mathrm{RT}}\left(\eta^{\mathrm{C}} - \eta_{\mathrm{eq}}^{\mathrm{C}}\right)\right) - \exp\left(-\frac{\alpha_{\mathrm{C}}^{\mathrm{C}} F}{\mathrm{RT}}\left(\eta^{\mathrm{C}} - \eta_{\mathrm{eq}}^{\mathrm{C}}\right)\right)\right) \tag{6}$$

where I_0^{Fe} is the exchange current density of iron deposition; $c_{\mathrm{ref}}^{\mathrm{Fe}^{+2}}$ is the reference concentration for Fe^{+2} ions; and η^{C} is the potential difference at the cathode electrode/electrolyte interface. The equilibrium potential for reaction (5) is

$$\eta_{\mathrm{eq}}^{\mathrm{C}} = E_0^{\mathrm{C}} + \frac{\mathrm{RT}}{n_e^{\mathrm{C}} F} \ln\left(\left(a_{\mathrm{C}}^{\mathrm{Fe}^{+2}}\right)^2\right) \tag{7}$$

Simultaneously with electrochemical reaction (5), the hydrogen evolution reaction occurs at the cathode electrode

$$2H_2O + 2e^- \rightarrow H_2 + 2OH^- \quad \left(E_0^{\mathrm{H}_2} = -0.83 \text{ V vs. SHE}\right) \tag{8}$$

The rate of hydrogen evolution is [15]

$$I^{\mathrm{H}_2} = I_0^{\mathrm{H}_2} \left(\frac{P^{\mathrm{H}_2}}{P_{\mathrm{ref}}^{\mathrm{H}_2}}\right)^{0.5} \left(\exp\left(\frac{\alpha_{\mathrm{A}}^{\mathrm{H}_2} F}{\mathrm{RT}}\left(\eta^{\mathrm{C}} - \eta_{\mathrm{eq}}^{\mathrm{H}_2}\right)\right) - \exp\left(-\frac{\alpha_{\mathrm{C}}^{\mathrm{H}_2} F}{\mathrm{RT}}\left(\eta^{\mathrm{C}} - \eta_{\mathrm{eq}}^{\mathrm{H}_2}\right)\right)\right) \tag{9}$$

where $I_0^{\mathrm{H}_2}$ is the exchange current density of hydrogen evolution; P^{H_2} is the partial pressure of hydrogen; and $P_{\mathrm{ref}}^{\mathrm{H}_2}$ is the reference pressure of hydrogen. The equilibrium potential for reaction (8) is

$$\eta_{\mathrm{eq}}^{\mathrm{H}_2} = E_0^{\mathrm{H}_2} - \frac{\mathrm{RT}}{n_e^{\mathrm{H}_2} F} \ln\left(a_{\mathrm{C}}^{\mathrm{OH}^-}\right) \tag{10}$$

The hydrogen evolution affects the current efficiency of iron deposition process at the cathode electrode. The partial current density of cathode electrochemical reaction (5) and (8) is taken into account in charge balance at the cathode electrode/electrolyte interface (Table 2). Electrochemical parameters of cathode and anode electrochemical reactions are listed in Table 3.

3.3 Combined chemical reactions

For the suspension flow in a parallel-plate electrochemical reactor, the source term in the suspension balance equation describes the partial dissolution of solid particles in alkaline media. The rate of partial dissolution of solid particles is defined by mass transfer equation

$$\Gamma_{\mathrm{d}} = M_{\mathrm{Fe}} \beta_{\mathrm{f,L}} a_{\mathrm{v}} \left(c_{\mathrm{eq}}^{\mathrm{Fe(OH)}_4^-} - c^{\mathrm{Fe(OH)}_4^-}\right) \tag{11}$$

where $\beta_{\mathrm{f,L}}$ is the empirical coefficient for mass transfer in liquid phase; a_{v} is the interfacial area of particles in suspension; and M_{Fe} is the molecular weight of $Fe(OH)_4^-$ ions. The distribution of local $Fe(OH)_4^-$ ions concentration is defined by diluted species conservation equation (Table 1). The equilibrium concentration of $Fe(OH)_4^-$ ions is defined by dissociation reaction of α-Fe_2O_3 in alkaline solution [16]

$$0.5\alpha - Fe_2O_3 + 2.5\,H_2O = Fe(OH)_4^- + H^+ \tag{12}$$

Auxiliary equations for calculating mass transfer coefficient and interfacial area are given in Appendix 2. The driving force for the dissolution process is a difference between equilibrium and local $Fe(OH)_4^-$ ions concentration. The distribution of $Fe(OH)_4^-$ ions is described by conservation equation for diluted species taking into account convection, diffusion, and migration processes in liquid phase of suspension (Table 1). The influence of the dissolution process is taken into account through the source term in the species balance equation $r^{\mathrm{Fe(OH)}_4^-} = \Gamma_{\mathrm{d}}/M_{\mathrm{Fe}}$. The necessary condition for partial dissolution of solid particles is that equilibrium concentration is higher than local concentration of $Fe(OH)_4^-$ ions. Equilibrium concentration of $Fe(OH)_4^-$ ions is a function of H^+ ions concentration as evidenced by the definition of dissociation constant for α-Fe_2O_3 particles in alkaline solution (Appendix 2). Negative source term Γ_{d} in balance equation for solid phase is responsible for the decrease of volume

Table 3 Electrochemical parameters for parallel-plate reactor

Parameter	Anode reaction (1)	Cathode reaction (5)	Cathode reaction (8)
Exchange current density I_0 (A m^{-2})	0.26	3.8	0.04
Reference concentration $c_{\text{ref}}^{\text{OH}^-}$ (mol m^{-3})	5	5	–
Reference concentration $c_{\text{ref}}^{\text{Fe(OH)}_4^-}$ (mol m^{-3})	–	3.72×10^{-3}	–
Reference pressure P_{ref} (atm)	–	–	1
Charge transfer coefficient α_A	0.5	0.5	0.5
Charge transfer coefficient α_C	0.5	0.5	0.5

fraction of solid phase. Positive source term $r^{\text{Fe(OH)}_4^-}$ in the species balance equation is responsible for the increase of Fe(OH)_4^- local concentration in liquid phase. The combined processes of chemical and electrochemical reactions are revealed through coupling the source term of partial dissolution process and interfacial mass transfer in the species balance equation.

Fe(III) ions participate in hydrolysis reactions given by Blesa and Matijević [17]

$$\text{Fe}^{+3} + \text{H}_2\text{O} \leftrightarrow \text{Fe(OH)}^{+2} + \text{H}^+ \tag{13}$$

$$\text{Fe(OH)}^{+2} + \text{H}_2\text{O} \leftrightarrow \text{Fe(OH)}_2^{+} + \text{H}^+ \tag{14}$$

$$2\text{Fe}^{+3} + 2\text{H}_2\text{O} \leftrightarrow \text{Fe}_2\text{(OH)}_2^{+4} + 2\text{H}^+ \tag{15}$$

Fe(II) hydrolysis reactions are

$$\text{Fe}^{+2} + \text{H}_2\text{O} \leftrightarrow \text{Fe(OH)}^{+1} + \text{H}^+ \tag{16}$$

$$\text{Fe(OH)}^{+1} + \text{H}_2\text{O} \leftrightarrow \text{Fe(OH)}_2 + \text{H}^+ \tag{17}$$

$$\text{Fe(OH)}_3^- + \text{H}_2\text{O} \leftrightarrow \text{Fe(OH)}_4^{-2} + \text{H}^+ \tag{18}$$

The experimental data [11, 17] on Fe(III) hydrolysis and ions stability indicate that the main form of hydrolyzed Fe(III) is Fe(OH)_4^- ion in alkaline solution. For convenience, the concentration dependence in cathode electrochemical reaction rate (6) is written for Fe(OH)_4^- ions. The equilibrium concentration of Fe(OH)_4^- ions in liquid phase is calculated using the dissociation constant for reaction (12) as shown in Appendix 2. The distribution of α-Fe_2O_3 particles in suspension is taken into account through volume fraction of the dispersed solid phase.

4 Cell voltage

For a parallel-plate electrochemical reactor operating under galvanostatic mode ($I_{\text{cell}} = \text{const}$), the cell voltage averaged over electrode surface is calculated as follows

$$V_{\text{avg}}^{\text{cell}} = E_{0,\text{avg}} + \eta_{\text{avg,act}}^{\text{A}} - \eta_{\text{avg,act}}^{\text{C}} + I_{\text{cell}} R_{\text{avg}}^{\text{E}} \tag{19}$$

where $\eta_{\text{avg,act}}^{\text{A}}$ is the anode activation overvoltage averaged over electrode surface; $\eta_{\text{avg,act}}^{\text{C}}$ is the cathode activation overvoltage averaged over electrode surface; and $R_{\text{avg}}^{\text{E}}$ is the ohmic resistance averaged over electrochemical reactor volume. The reversible cell potential is given by Nernst equation

$$E_0 = \left(E_0^{\text{A}} - E_0^{\text{C}}\right) + \frac{\text{RT}}{n_e F} \ln\left(\frac{\left(a_{\text{C}}^{\text{Fe}^{+2}}\right)^2}{\left(a_{\text{A}}^{\text{OH}^-}\right)^4}\right). \tag{20}$$

5 Electrolyte conductivity

Liquid phase of suspension contains Fe(OH)_4^- ions, hydrogen ions H^+, sodium ions Na^+, and hydroxyl ions OH^-. The overall suspension conductivity is a function of temperature, volume fraction of solid particle, and ion species concentrations. Cruz et al. [18] proposed application of Maxwell's model on conductivity in heterogeneous media for estimating the overall suspension conductivity

$$\frac{k_{\text{s}}}{k_{\text{L}}} = \frac{2k_{\text{L}} + k_{\text{p}} - 2\left(k_{\text{L}} - k_{\text{p}}\right)\varepsilon_{\text{d}}}{2k_{\text{L}} + k_{\text{p}} + \left(k_{\text{L}} - k_{\text{p}}\right)\varepsilon_{\text{d}}} \tag{21}$$

where k_{s} is the overall suspension conductivity; k_{L} is the conductivity of the suspending liquid; and k_{p} is the conductivity of a disperse phase of spherical particles. The conductivity of a disperse phase k_{p} is a function of external electrolyte and pore electrolyte. Conductivity of spherical particles can be estimated by technique proposed by Kastening et al. [19]. Electrolyte conductivity is linked to ions mobilities [20]

$$k_{\text{L}} = F^2 \sum_{m=1} \left(z^{(m)}\right)^2 u^{(m)} c^{(m)} \tag{22}$$

where $u^{(m)}$ is the ion mobility of m-species and $z^{(m)}$ is the charge number of m-species. Mobilities of ions are taken from [21]. Mobility of Fe(OH)_4^- ions is set equal to Fe^{+3} ions.

Molar concentration of Na^+ ions is calculated from electroneutrality condition

$$\sum_{m=1} z^{(m)} c^{(m)} = 0. \quad (23)$$

Overall averaged suspension resistance is

$$R^{E}_{avg} = \frac{\delta_E}{k_{avg,s}}, \quad (24)$$

where $k_{avg,s}$ is the overall suspension conductivity averaged over parallel-plate reactor volume.

6 Results and discussion

To validate the model we used experimental data reported by Allanore et al. [4] for α-Fe_2O_3 suspension electrolysis in a parallel-plate electrochemical reactor. Allanore et al. used experimental setup including a horizontal parallel-plate cell, centrifugal pump, a perfectly mixed storage tank, and a magnetic flow meter. The circulation rate was controlled by means of a centrifugal pump and a magnetic flow meter. Suspension flow was fed to the parallel-plate electrochemical reactor from the mixing tank. Outlet flow from the parallel-plate reactor was returned to the mixing tank. Assuming that the residence time of the electrolyte in the mixed storage tank is sufficient for suspension to reach equilibrium in the partial dissolution, species concentration at the inlet section is set equal to the equilibrium concentration in the suspension. Operating conditions and geometry parameters of parallel-plate electrochemical reactor are listed in Table 4. The inlet species concentration is specified taking into account the equilibrium partial dissolution of solid particles and the degree of NaOH dissociation as shown in Appendix 2.

For solid particles suspended in liquid flow, partial dissolution is defined by mass transfer equation in liquid phase. The rate of interfacial mass transfer from solid–liquid interface to the liquid phase (11) is a function of volumetric mass transfer coefficient and driving force for mass transfer. The volumetric mass transfer coefficient is calculated taking into account local mass transfer from the suspended particle to the bulk of liquid phase and interfacial area of particles in the suspension (Appendix 2).

Allanore et al. [4] used experimental setup including a horizontal parallel-plate electrochemical reactor with the flow rates ranging from 1 to 400 L h^{-1} in experiments. The corresponding Reynolds number ranged from $Re_L = 6$ to 1600. For testing the developed parallel-plate electrochemical reactor model, we used minimal and maximal values of flow rates from operating conditions. Comparison of velocity profiles in Fig. 3 with analytical solution [22] indicates that velocity profile in parallel-plate reactor at

Table 4 Operating conditions for parallel-plate reactor

Parameter	Value	Ref.
50 % NaOH flow rate (l h^{-1})	1[a]; 150[b]	[4]
Reynolds number Re_L	6[a]; 1600[b]	Calc.
Suspension volume fraction ε_d	0.13	[4]
Particle size d_p (μm)	10	[4]
NaOH dissociation constant α	0.002	Calc.
Inlet concentration $c_{in}^{Na^+}$ (mol m^{-3})	37	Calc.
Inlet concentration $c_{in}^{OH^-}$ (mol m^{-3})	37	Calc.
Inlet concentration $c_{in}^{Fe(OH)_4^-}$ (mol m^{-3})	3.72×10^{-3}	Calc.
Temperature (°C)	100	[4]
Cell current density I_{cell} (A m^{-2})	1000	[4]
Cell area (cm^2)	21	[4]
Electrode length L (cm)	7	[4]
Electrode width B (cm)	3	[4]
Distance between electrodes δ_E (cm)	1	[4]
Mass transfer coefficient $\beta_{f,L}$ (m s^{-1})	3×10^{-6}	Calc.

[a] $Re_L = 6$

[b] $Re_L = 1600$

$Re_L = 1600$ corresponds to the entrance region of a rectangular channel. Outlet velocity profile in parallel-plate reactor at $Re_L = 6$ is close to the analytical solution corresponding to the fully developed laminar flow in the rectangular channel.

The profile of the dispersed phase content in Fig. 4 indicates the effect of partial dissolution processes on the distribution. The influence of the dispersed phase is revealed through the interfacial area in interfacial source term describing the partial dissolution process in the species balance equation. The interfacial area is proportional to the volume fraction of the dispersed phase. Decrease in the suspension volume fraction leads to the drop in the additional component flux due to the dissolution process. Adsorption of particles on the cathode electrode surface is taken into account through setting volume fraction of dispersed phase equal to the maximal particles packing value at the boundary. A high rate of mass transfer from the dispersed solid phase to the continuous liquid phase is achieved in the partial dissolution due to the high interfacial area of particles. The volume fraction of solid particles is decreased in the suspension flow due to the partial dissolution of α-Fe_2O_3 particles in alkaline media.

The electrolyte current density is linked to the electrode current density through boundary condition of charge balance written for potential differences at the electrolyte/electrode interface (Table 2). The partial current density of iron deposition shown in Fig. 5 is a function of $Fe(OH)_4^-$ ions concentration and potential difference as specified by Butler–Volmer equation for cathode electrochemical reaction (5). The total current density profile at

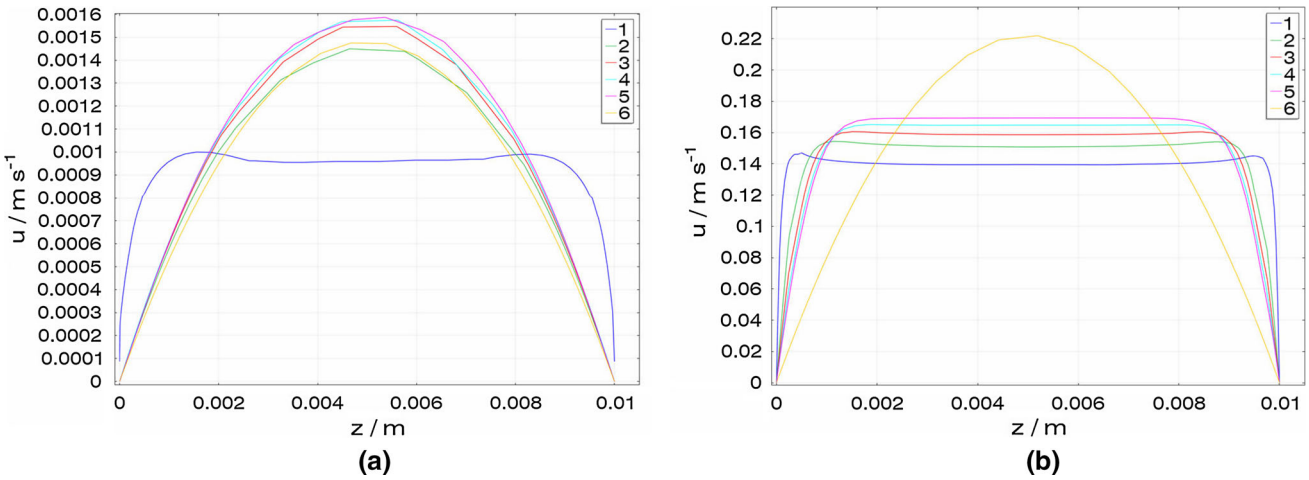

Fig. 3 Velocity profile in liquid phase of suspension in parallel-plate reactor for Reynolds number $Re_L = 6$ (**a**) and $Re_L = 1600$ (**b**). *1* Plane $x = 0.0017$ m intersecting plane $y = B/2$, *2* plane $x = 0.017$ m intersecting plane $y = B/2$, *3* plane $x = 0.034$ m intersecting plane $y = B/2$, *4* plane $x = 0.051$ m intersecting plane $y = B/2$, *5* plane $x = 0.068$ m intersecting plane $y = B/2$, *6* analytical solution [22]

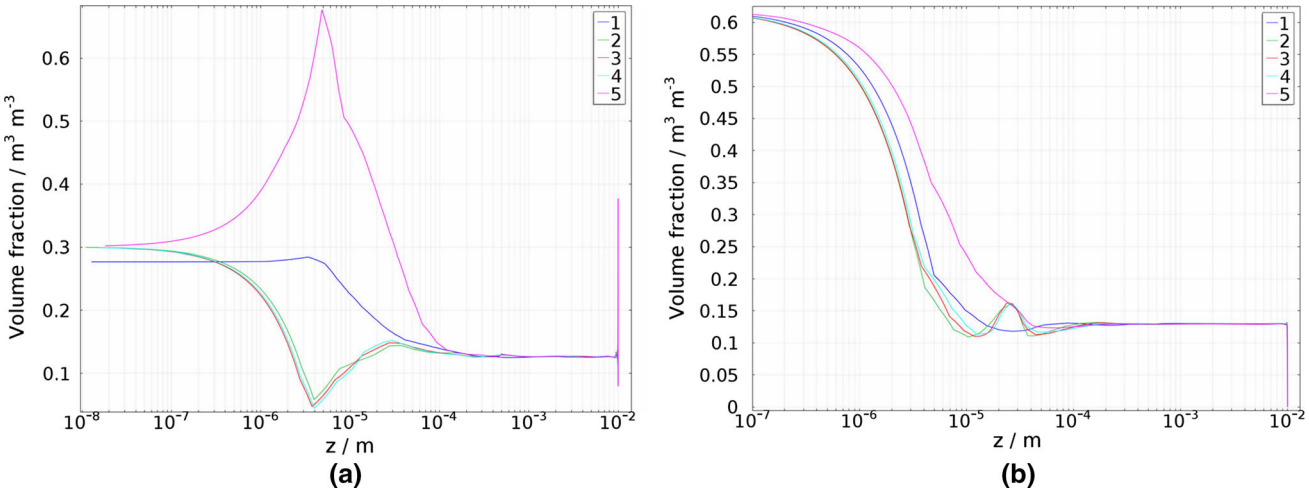

Fig. 4 Dispersed phase profiles in two-phase flow in parallel-plate reactor for suspension electrolysis at Reynolds number $Re_L = 6$ (**a**) and $Re_L = 1600$ (**b**). *1* Plane $x = 0.0017$ m intersecting plane $y = B/2$, *2* plane $x = 0.017$ m intersecting plane $y = B/2$, *3* plane $x = 0.034$ m intersecting plane $y = B/2$, *4* plane $x = 0.051$ m intersecting plane $y = B/2$, *5* plane $x = 0.068$ m intersecting plane $y = B/2$

the cathode electrode surface is the sum of partial current densities of iron deposition (Fig. 5) and hydrogen evolution (Fig. 6). The mixed potential of the cathode electrochemical reactions is taken into account in boundary condition for charge balance at the cathode electrode/electrolyte interface (Table 2).

The current density profile at the anode electrode surface in Fig. 7 is a function of OH^- ions distribution and potential difference in accord with the Butler–Volmer equation for anode electrochemical reaction (1). The cell voltage is taken into account through the boundary condition for electrolyte potential at the anode electrode/electrolyte interface.

Distribution of the electrolyte potential profile in Fig. 8 reflects the interaction between mass transfer and combined electrochemical and chemical reactions in the parallel-plate reactor. The effect of electrochemical reaction on the electrolyte potential profile is revealed through the boundary condition for electrolyte phase potential related to the potential difference at the electrode/electrolyte interface (Table 2). The distribution of the electrolyte potential is affected by conductivity of suspension and species distribution in liquid phase.

The electrolyte conductivity is a function of the ions concentrations in liquid phase and volume fraction of solid particles in the suspension. Electrolyte conductivity profile

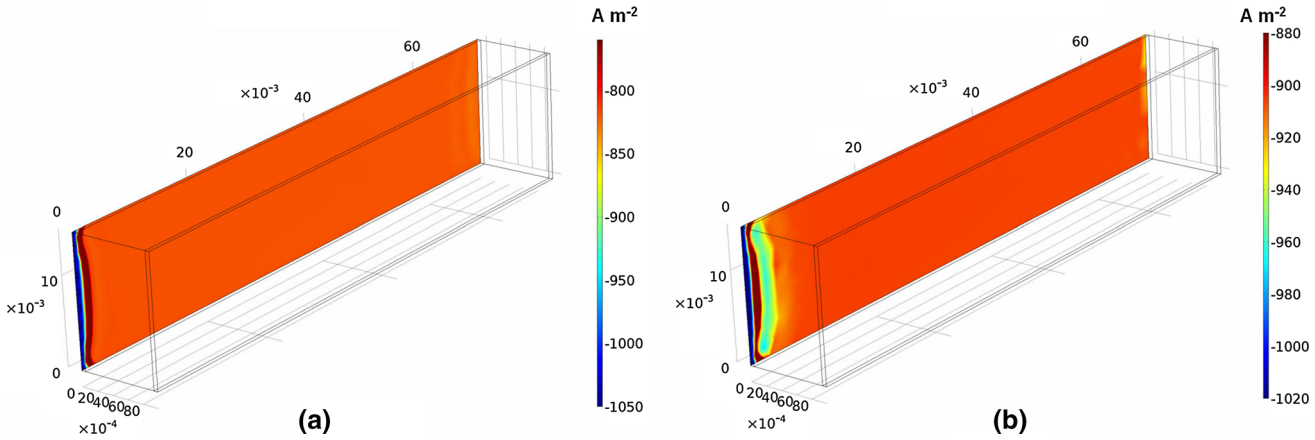

Fig. 5 Partial current density profile corresponding to the electrochemical reaction of iron deposition at the cathode electrode for suspension electrolysis in parallel-plate reactor. **a** Reynolds number $Re_L = 6$; **b** Reynolds number $Re_L = 1600$

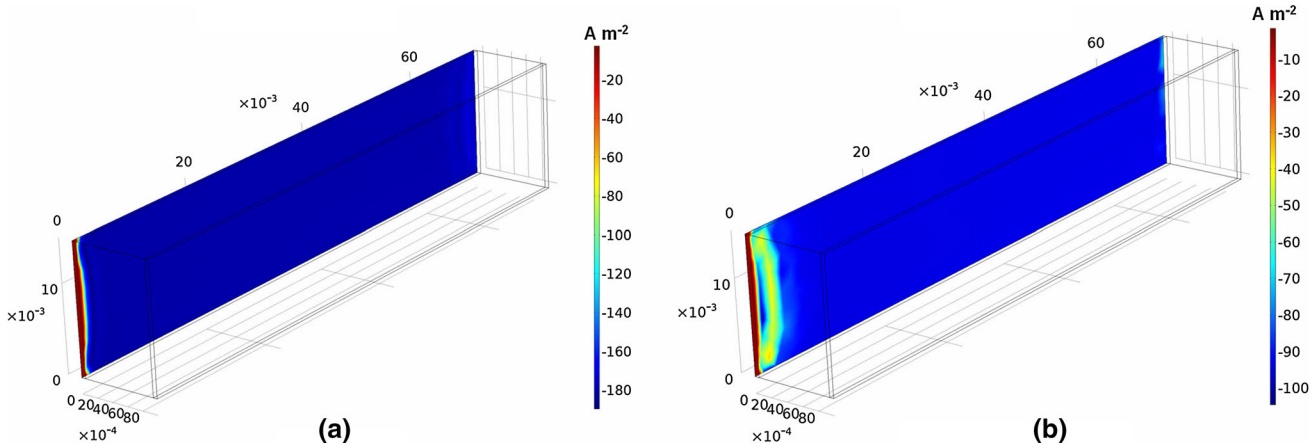

Fig. 6 Partial current density profile due to hydrogen evolution at the cathode electrode in parallel-plate reactor (PPR) in suspension electrolysis. **a** Reynolds number $Re_L = 6$; **b** Reynolds number $Re_L = 1600$

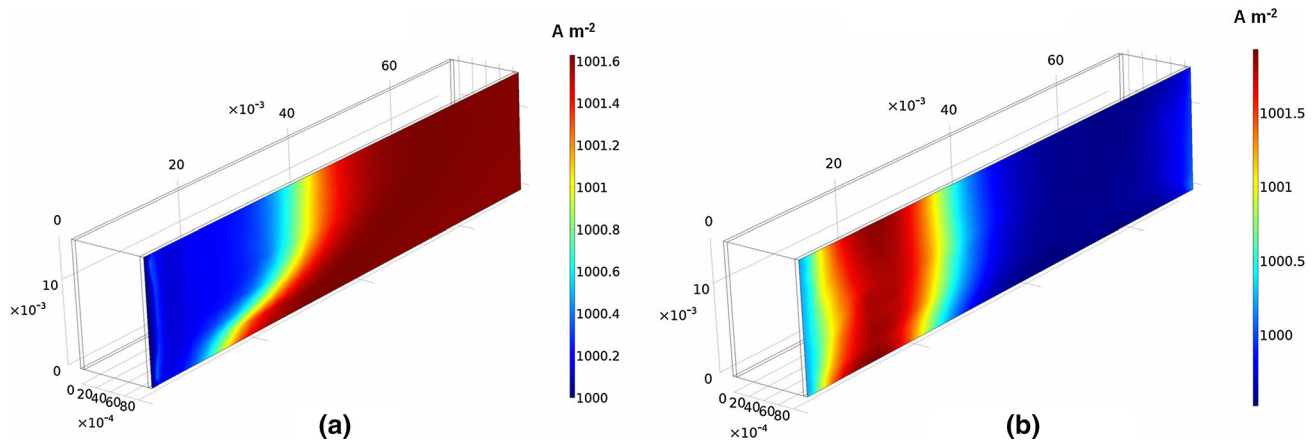

Fig. 7 Current density profile at the anode electrode for suspension electrolysis in parallel-plate reactor. **a** Reynolds number $Re_L = 6$; **b** Reynolds number $Re_L = 1600$

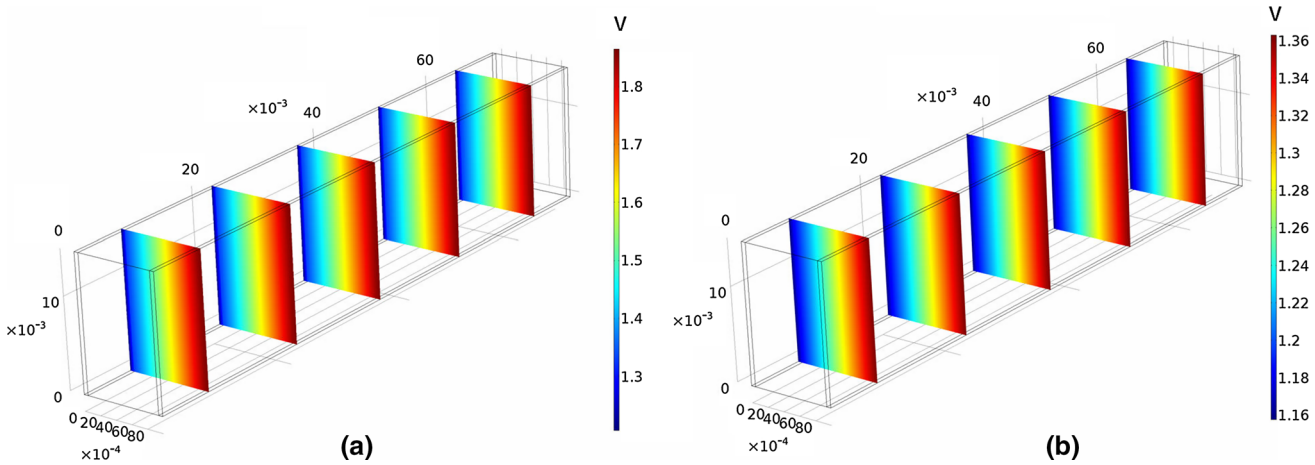

Fig. 8 Electrolyte potential profiles for suspension electrolysis in parallel-plate reactor. **a** Reynolds number $Re_L = 6$; **b** Reynolds number $Re_L = 1600$

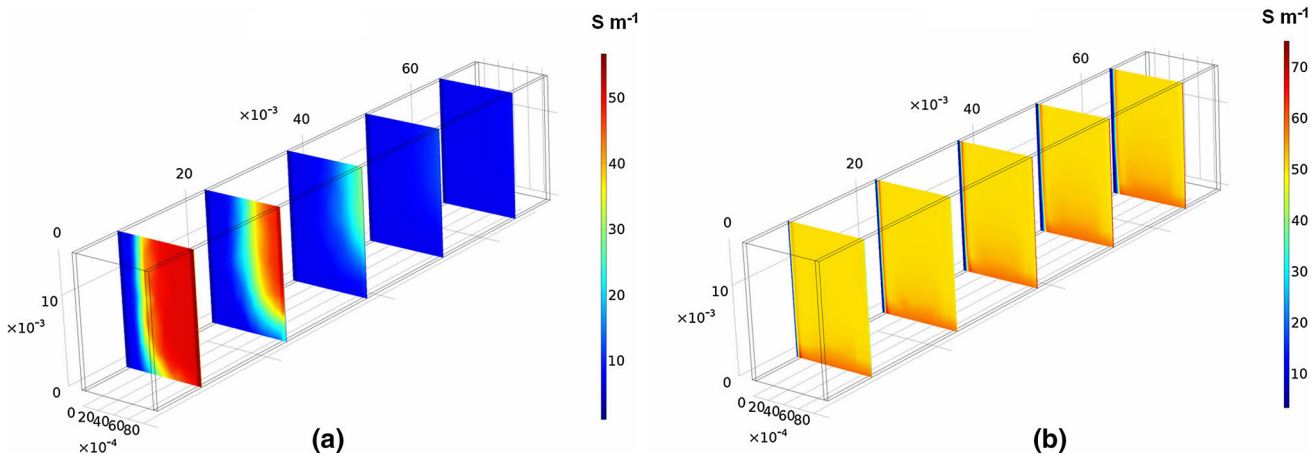

Fig. 9 Distribution of electrolyte conductivity for suspension electrolysis in parallel-plate reactor. **a** Reynolds number $Re_L = 6$; **b** Reynolds number $Re_L = 1600$

in Fig. 9 reflects the influence of ions concentration on the distribution. The conductivity distribution follows the OH^- ions profile in liquid phase. The maximal value of the electrolyte conductivity corresponds to the region with high OH^- ions concentration.

Numerical analysis is carried out for suspension electrolysis taking into account momentum, mass, and charge transfer in two-phase flow in the parallel-plate electrochemical reactor. The variation of ions concentration and current density at the electrode interface indicates the interaction between transfer processes to be in accord with the given boundary conditions (Table 2). The species concentration at the interface depends on the transfer processes in liquid electrolyte between parallel electrodes including migration of ions due to the electrolyte potential profile. The $Fe(OH)_4^-$ ions participate in cathode electrochemical reaction as a reactant together with chemical reaction of dissolution as a product. The OH^- ions participate in cathode electrochemical reaction as a product together with anode electrochemical reaction as a reactant. The Na^+, H^+, and ions migrate from anode electrode to the cathode electrode. The $Fe(OH)_4^-$ and OH^- ions migrate from cathode electrode to the anode electrode due to the electrolyte potential profile.

A distinctive feature of suspension electrolysis is an additional species flux due to the partial dissolution of the dispersed solid phase (particles). The effect of increasing suspension electrolyte flow rate is to increase the concentration of OH^- ions and to intensify the partial dissolution of solid particles in electrolyte as shown in Fig. 10.

Hydrogen ion concentration at the cathode electrode surface is defined by equilibrium electrochemical reaction of the dissolved hydrogen oxidation. Equilibrium concentration of hydrogen ion is calculated from Nernst equation

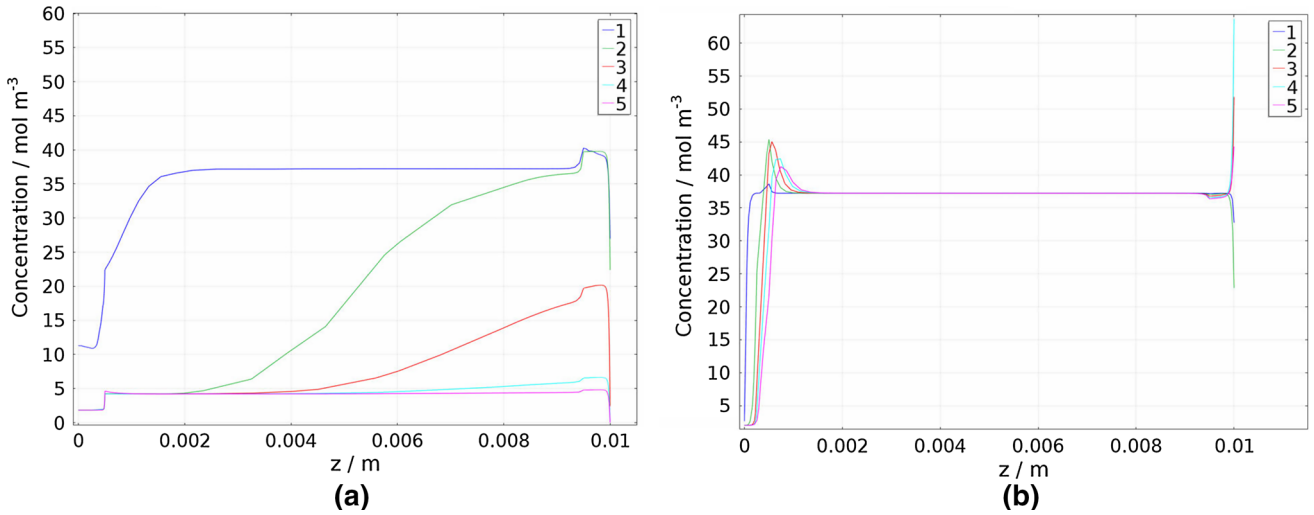

Fig. 10 Concentration profiles of OH^- ions in liquid phase for suspension electrolysis in parallel-plate reactor at Reynolds number $Re_L = 6$ (**a**) and $Re_L = 1600$ (**b**). *1* plane $x = 0.0017$ m intersecting plane $y = B/2$, *2* plane $x = 0.017$ m intersecting plane $y = B/2$, *3* plane $x = 0.034$ m intersecting plane $y = B/2$, *4* plane $x = 0.051$ m intersecting plane $y = B/2$, *5* plane $x = 0.068$ m intersecting plane $y = B/2$

(Appendix 2). For electrowinning processes, the pH value is changed from 2 to 16 depending on the cathode electrode potential [23].

Combination of chemical and electrochemical processes afforded a significant increase in performance of the electrochemical reactor. The intensification of transfer processes is achieved in suspension electrolysis due to the acceleration of combined processes when reactant of electrochemical reaction is a product of chemical reaction of partial dissolution. The $Fe(OH)_4^-$ ions participate in the cathode electrochemical reaction parallel with the chemical reaction of partial dissolution of α-Fe_2O_3 particles. As evidenced by the definition of dissociation constant for α-Fe_2O_3 particles in alkaline media, the partial dissolution of the solid particles is increased with pH of the electrolyte. The change of the local pH value induces the displacement of dissociation equilibrium of α-Fe_2O_3 particles in alkaline media. As can be seen in Fig. 11, local region near the cathode surface ($z = 0$) with low concentration of hydrogen ions is suitable for dissolving solid particles due to the high driving force of mass transfer.

The distribution of $Fe(OH)_4^-$ ions depends on the diffusion and migration processes in liquid phase together with the electrochemical reaction at the cathode surface and partial dissolution of solid particles (Fig. 12). The concentration peak of $Fe(OH)_4^-$ ions near the cathode electrode is due to the superposition of electrochemical, chemical, and mass transfer processes. Chemical process of partial dissolution of particles gives a significant impact on the electrochemical reactor performance due to an additional $Fe(OH)_4^-$ ions flux increasing the rate of cathode electrochemical reaction of iron deposition.

The driving force for mass transfer in the partial dissolution process is the difference between local and equilibrium $Fe(OH)_4^-$ ions concentration. The equilibrium concentration of $Fe(OH)_4^-$ ions is a function of local pH value. The highest rate of partial dissolution is achieved in the region with high pH value (Figs. 13, 14). The local region near the cathode surface ($z = 0$) with positive driving force and source term corresponds to the region with predominate partial dissolution of α-Fe_2O_3 particles. The negative source term indicates the region with predominate partial crystallization of α-Fe_2O_3 particles from liquid phase.

Analysis of transfer processes in Figs. 11, 12, 13, and 14 indicates that electrochemical reaction of iron deposition at the cathode electrode is accompanied by chemical reaction of partial dissolution and crystallization of Fe_2O_3 particles in the local region near the cathode surface together with mass transfer due to the diffusion and migration processes. The effect of increasing the inlet flow rate is to increase the convective mass transfer and to intensify the partial dissolution of solid particles due to the combined processes of mass and charge transfer together with chemical and electrochemical reactions in suspension electrolysis.

Evolution of oxygen gas is governed by mass transfer and desorption of the dissolved oxygen from liquid phase to the gas phase. Simulation results reported in literature for electrolysis in a parallel-plate reactor indicates that gas content profile follows the dissolved gas component profile [24]. The maximal concentration of oxygen is achieved at the anode electrode/electrolyte interface. The limiting gas content can be evaluated using equilibrium flash equation

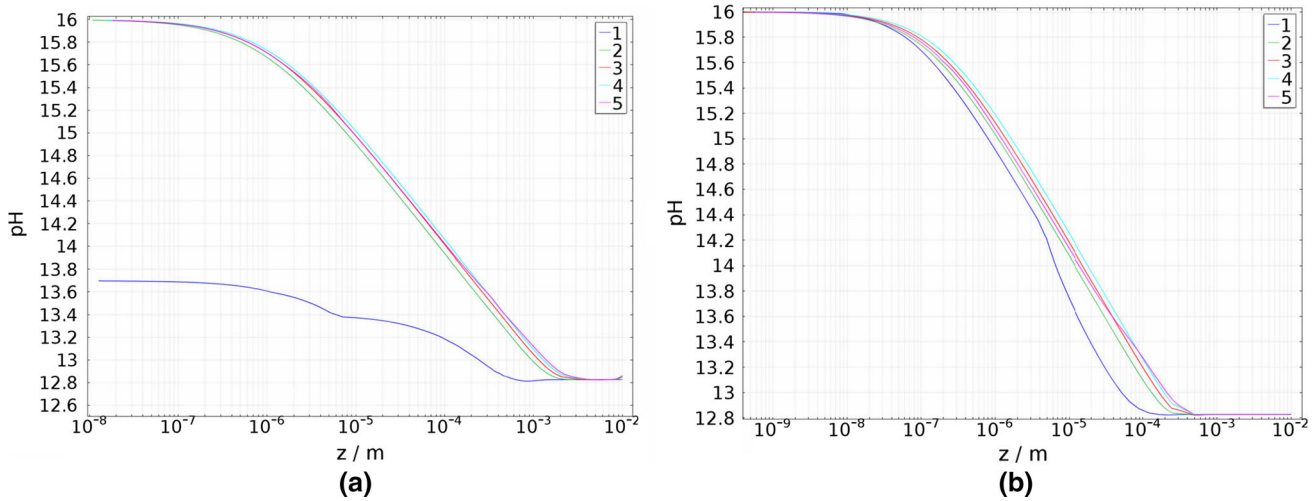

Fig. 11 pH profiles in liquid phase for suspension electrolysis in parallel-plate reactor at Reynolds number $Re_L = 6$ (**a**) and $Re_L = 1600$ (**b**). *1* plane $x = 0.0017$ m intersecting plane $y = B/2$, *2* plane $x = 0.017$ m intersecting plane $y = B/2$, *3* plane $x = 0.034$ m intersecting plane $y = B/2$, *4* plane $x = 0.051$ m intersecting plane $y = B/2$, *5* plane $x = 0.068$ m intersecting plane $y = B/2$

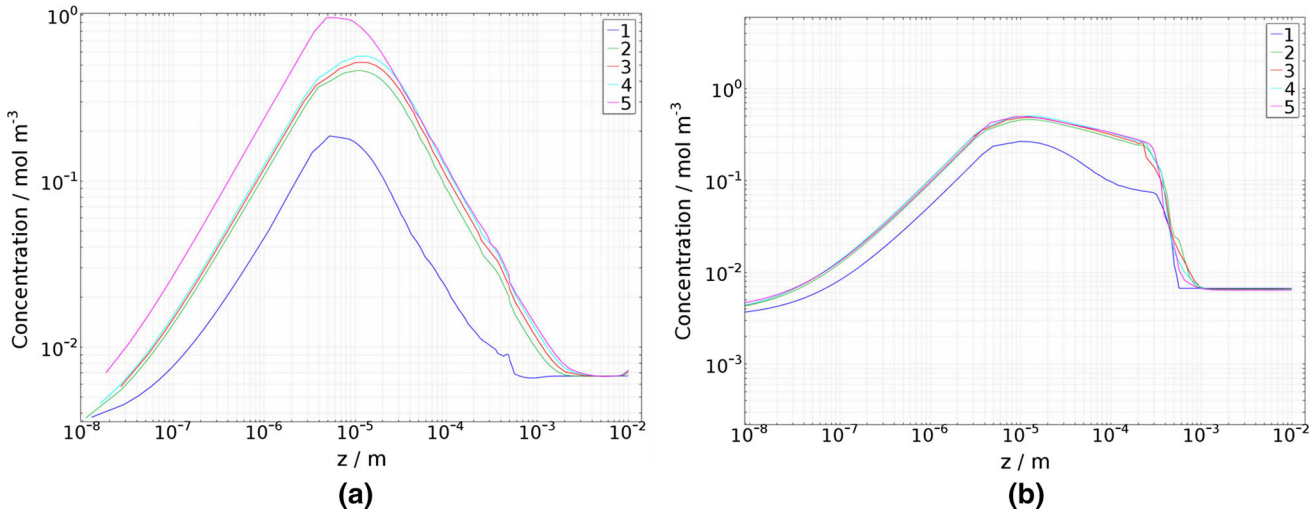

Fig. 12 Concentration profiles of $Fe(OH)_4^-$ ions in liquid phase for suspension electrolysis in parallel-plate reactor at Reynolds number $Re_L = 6$ (**a**) and $Re_L = 1600$ (**b**). *1* Plane $x = 0.0017$ m intersecting plane $y = B/2$, *2* plane $x = 0.017$ m intersecting plane $y = B/2$, *3* plane $x = 0.034$ m intersecting plane $y = B/2$, *4* plane $x = 0.051$ m intersecting plane $y = B/2$, *5* plane $x = 0.068$ m intersecting plane $y = B/2$

(Appendix 2). For parallel-plate electrochemical reactor under the given operating conditions, the limiting gas content $\alpha_G \approx 0.1$ is observed at the anode electrode surface. The dissolved hydrogen concentration and gas content at the cathode electrode surface is less than those values at the anode electrode in proportion to the component flux. The influence of gas content is revealed through the increase of overvoltage due to the decrease of electrode surface and drop of gas–liquid flow conductivity. Rough estimate indicates that the effect of gas content on physical properties and conductivity is negligible under the given operating conditions. Table 5 gives the comparison of the output simulation results with the experimentally measured values reported by Allanore et al. [4].

The difference between simulations and experimental results can be explained by idealization of interfacial transfer processes in suspension electrolysis. Iron deposition at the cathode together with α-Fe_2O_3 partial dissolution and crystallization processes near the electrode surface leads to a multiple redistribution of the porosity and interfacial area profiles. Further modification of the electrochemical reactor model is possible using population

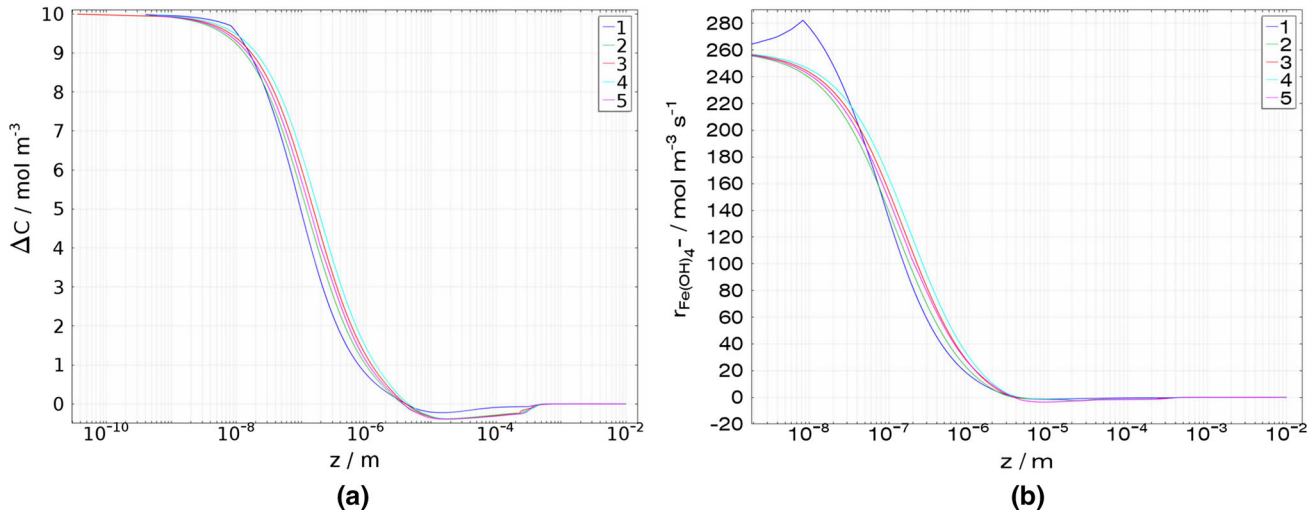

Fig. 13 Driving force for mass transfer $\Delta c = c_{eq}^{Fe(OH)_4^-} - c^{Fe(OH)_4^-}$ (**a**) and Fe_2O_3 dissolution rate (**b**) profiles for suspension electrolysis in parallel-plate reactor. Reynolds number $Re_L = 1600$. *1* Plane $x = 0.0017$ m intersecting plane $y = B/2$, *2* plane $x = 0.017$ m intersecting plane $y = B/2$, *3* plane $x = 0.034$ m intersecting plane $y = B/2$, *4* plane $x = 0.051$ m intersecting plane $y = B/2$, *5* plane $x = 0.068$ m intersecting plane $y = B/2$

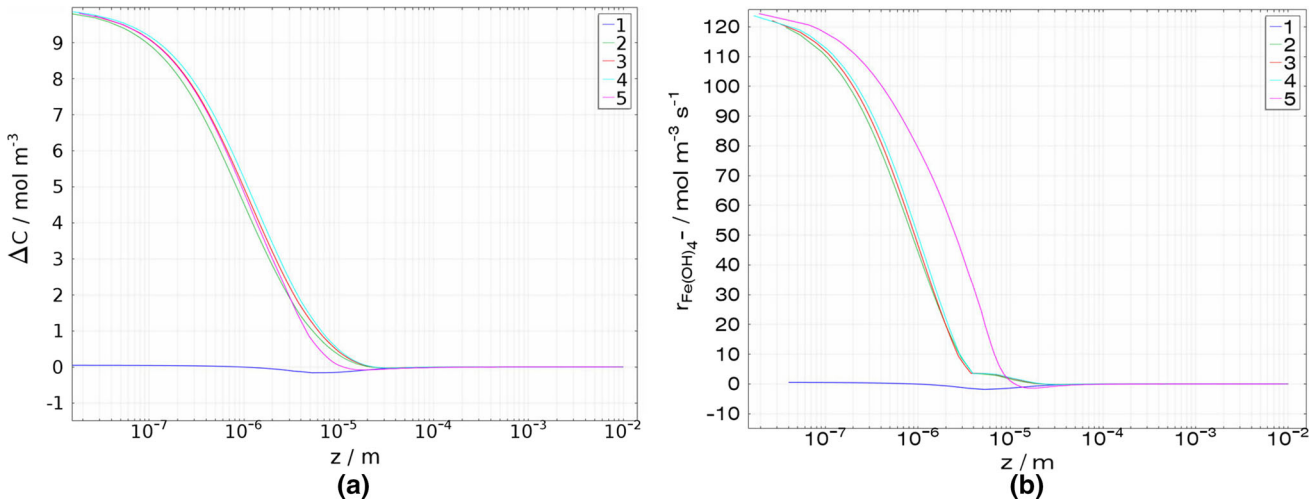

Fig. 14 Driving force for mass transfer $\Delta c = c_{eq}^{Fe(OH)_4^-} - c^{Fe(OH)_4^-}$ (**a**) and Fe_2O_3 partial dissolution rate (**b**) profiles for suspension electrolysis in parallel-plate reactor. Reynolds number $Re_L = 6$. *1* Plane $x = 0.0017$ m intersecting plane $y = B/2$, *2* plane $x = 0.017$ m intersecting plane $y = B/2$, *3* plane $x = 0.034$ m intersecting plane $y = B/2$, *4* plane $x = 0.051$ m intersecting plane $y = B/2$, *5* plane $x = 0.068$ m intersecting plane $y = B/2$

Table 5 Comparison of predicted values with experimental data [4] for $Re_L = 1600$

Parameter	Predicted	Experiment [4]
Cell voltage (V)	1.95	1.68
Current efficiency (%)	90.9	90.1
Conversion of solid particles (%)	8	2

balance equations taking into account particle size distribution together with death and birth of particles.

The drop in current efficiency (CE) with the decrease of dispersed phase volume fraction is associated with the drop in the interfacial area of particles participating in partial dissolution near the cathode electrode surface in the region with high pH value. The drop in the interfacial area results in a decrease of the impact of dissolution process on the

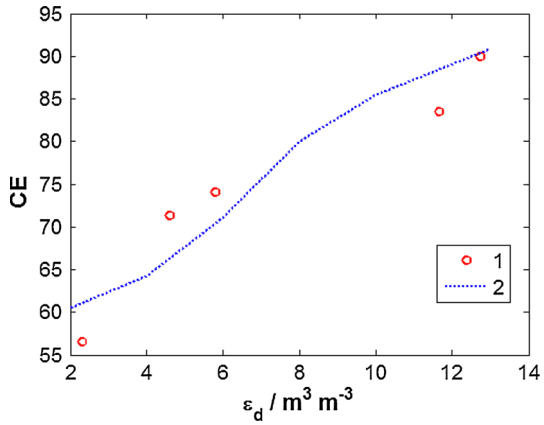

Fig. 15 Current efficiency of iron deposition at the cathode electrode in combined chemical and electrochemical processes. Suspension electrolysis in parallel-plate reactor. Reynolds number $Re_L = 1600$. *1* Experimental data [4], *2* parallel-plate reactor model

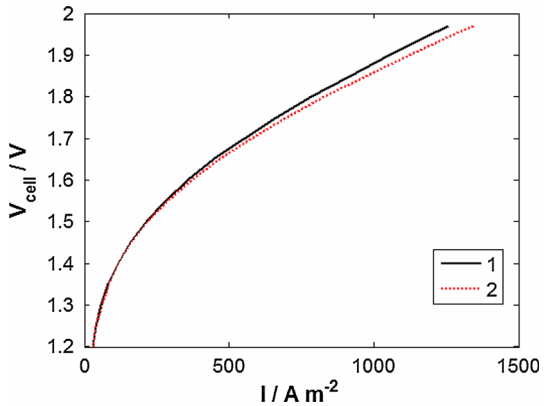

Fig. 16 The effect of distance δ_E between anode and cathode electrode on cell voltage for suspension electrolysis in parallel-plate reactor. Reynolds number $Re_L = 1600$. *1* $\delta_E = 1$ cm, *2* $\delta_E = 0.9$ cm

total species flux at the electrode/electrolyte interface reducing the partial current of iron deposition in the total cathode electrode current density (Fig. 15).

Conventional electrochemical processes in parallel-plate reactors are affected by flow rate, diffusion, and mass transfer processes. The effect of increasing the inlet flow rate is to increase the driving force for mass transfer from the bulk to the interface. Contrasting the performance of the electrochemical reactor against the minimal and maximal values of the inlet flow rates, we are able to identify the effect of the mass transfer on the process.

The basic contradiction of a parallel-plate electrochemical reactor is that the distance between anode and cathode electrode is limited by the performance of the reactor. Intensification of combined processes is feasible through intensification of momentum, mass, and charge transfer processes in a new electrochemical reactor design. A necessary condition for high performance combined processes is a minimal distance between anode and cathode electrode in a new electrochemical reactor. As evidenced by charge balance at electrode/electrolyte interface, electrode current density is equal to the electrolyte current density under the steady state condition. This implies that performance of electrochemical reactor is limited by the electrolyte current. For a linear membrane phase potential, electrolyte current can be calculated from voltage equation [25, 26]. Electrolyte current is a function of theoretical potential, activation overvoltages, and ohmic resistance. Reducing the distance between anode and cathode electrode, we are able to increase the electrolyte current due to the drop in cell resistance (Fig. 16).

Evaluating the limiting diffusion flux in the parallel-plate reactor, Allanore et al. [4] concluded that the operating current density (1000 A m^{-2}) in suspension electrolysis is higher than the predicted limiting current density (100 A m^{-2}). Observation of the total component mass balance in parallel-plate electrochemical reactor leads to the conclusion that the total ferric ions flow (100 %) reduced at the cathode electrode consists of 9 % diffusion component flow and 91 % component flow due to the partial dissolution of solid particles as shown in Fig. 17 for case study (b) with Reynolds number $Re_L = 1600$. Numerical results including ions concentration distribution, reaction, and mass transfer fluxes distribution are used for better understanding of transfer processes during the process.

According to the boundary condition, the concentration of the reacting species at the electrode surface is determined by the rate of electrochemical reaction and component flux at the interface including diffusion and dissolution processes. Simulation results indicate that the

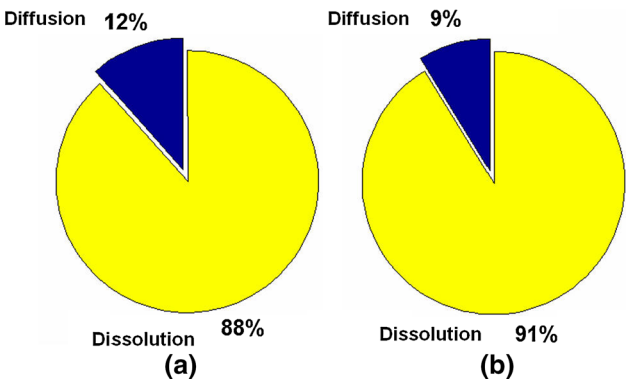

Fig. 17 Contribution of diffusion and dissolution processes to the iron deposition at the cathode electrode in combined chemical and electrochemical processes. Suspension electrolysis in parallel-plate reactor. **a** Reynolds number $Re_L = 6$; **b** Reynolds number $Re_L = 1600$

diffusion flux represents less than 20 % of the total species flux at the cathode electrode in suspension electrolysis. Dissolution of solid particles in liquid electrolyte phase near the cathode electrode produces an additional species flux dominating over the diffusion flux.

Combining chemical and electrochemical processes, we are able to intensify the transfer processes in α-Fe_2O_3 suspension electrolysis. The intensification is achieved due to the $Fe(OH)_4^-$ ions participating in electrochemical and chemical reactions. A decrease in $Fe(OH)_4^-$ ions concentration participating in electrochemical reaction as a reactant leads to the acceleration of chemical reaction of partial dissolution of solid particles with $Fe(OH)_4^-$ ions as a product of the chemical reaction. The high value of the dissolution rate is achieved due to the high value of mass transfer driving force and interfacial area of the solid particles in suspension electrolysis.

Further model development requires detailed description of interfacial momentum, mass, and charge transfer in multiphase electrochemical processes. The developed model is suitable for the numerical study of transfer processes in suspension electrolysis with different systems and electrochemical reactor designs.

7 Conclusions

A CFD model is developed for a parallel-plate electrochemical reactor taking into account combined chemical and electrochemical processes in suspension electrolysis. The influence of combined chemical and electrochemical processes is reflected through additional species flux due to the partial dissolution of the solid particles. It is shown that the main contribution to the deposition rate of iron can be attributed to the partial dissolution process of solid particles in suspension electrolysis. Numerical investigation indicates that further intensification of the combined processes is feasible through intensification of momentum, mass, and charge transfer processes in an electrochemical reactor.

Appendix 1: Charge balance at the electrode/electrolyte interface

The electric potential fields are governed by the charge conservation equations. The charge balance at interface between electron-conducting and ion conducting media is given by [27]

$$\frac{\partial Q}{\partial \tau} + \nabla \cdot I_s = (I_1 - I_2) \tag{A.1.1}$$

where I_1 is the current in electron-conducting media normal to the boundary; I_2 is the current in ion –conducting media normal to the boundary; I_s is the superficial current density; and Q is the charge. The interfaces between ionic and electronic media behave like a capacitor in which the charge density is a function of potential difference across the double layer. Charge or discharge rate at the electrode–electrolyte double layer can be defined as

$$\frac{\partial Q}{\partial \tau} = C_{dl}\frac{\partial \eta}{\partial t} \tag{A.1.2}$$

where η is the potential differences, $\eta = \varphi - \varphi_m$. For the potential difference at the electrode/electrolyte interface, the following charge conservation equation is valid

$$C_{dl}\frac{\partial \eta}{\partial \tau} = -\nabla \cdot I_s + (I_1 - I_2). \tag{A.1.3}$$

Appendix 2: Auxiliary equations for combined processes

The dissociation reaction of α-Fe_2O_3 in alkaline solution is given by Diakonov et al. [16]

$$0.5Fe_2O_3 + 2.5H_2O = Fe(OH)_4 + H^+ \tag{A.2.1}$$

The dissociation constant is defined as

$$K_s = a_{Fe(OH)_4^-} a_{H^+} \tag{A.2.2}$$

where $a_{Fe(OH)_4^-}$ is the activity of $Fe(OH)_4^-$ ions and a_{H^+} is the activity of H^+ ions. The equilibrium concentration of $Fe(OH)_4^-$ ions is a function of H^+ ions concentration

$$a_{Fe(OH)_4^-} = K_s / a_{H^+}. \tag{A.2.3}$$

Activity of species is associated with the molar concentration $a = 0.001\gamma c$, where γ is the activity coefficient. The activity coefficient is calculated using NBS smoothed experimental data [28]. The ionic association in NaOH solution is given by

$$Na^+ + OH^- \leftrightarrow NaOH \tag{A.2.4}$$

The association constant is

$$K_A = \frac{(1-\alpha)c^{NaOH}}{(\alpha c^{NaOH}\gamma^{OH^-})^2} \tag{A.2.5}$$

where c^{NaOH} is the molar concentration of NaOH solution; α is degree of dissociation; and γ^{OH^-} is activity coefficient of OH^- ions. The constant of association for 50 % NaOH solution is taken from [29]. The degree of dissociation is found from solving (A.2.5) under the given electrolyte concentration. The inlet concentration of OH^- and Na^+

ions is calculated using the degree of electrolyte dissociation

$$c_{\text{in}}^{\text{OH}^-} = c^{\text{NaOH}} \cdot \alpha,\ c_{\text{in}}^{\text{Na}^+} = c_{\text{in}}^{\text{OH}^-}. \tag{A.2.6}$$

The inlet concentration of Fe(OH)_4^- ions is set equal to the equilibrium concentration $c_{\text{in}}^{\text{Fe(OH)}_4^-} = 1000 \cdot a^{\text{Fe(OH)}_4^-}$. The next Nernst equation is valid for equilibrium electrochemical reaction (4)

$$E = E^0 + \frac{\text{RT}}{zF} \ln\left(\frac{a^{\text{Fe}^{+3}}}{a^{\text{Fe}^{+2}}}\right)$$

or

$$a^{\text{Fe}^{+2}} = a^{\text{Fe}^{+3}} \exp\left(-\frac{zF}{\text{RT}}\left(E - E^0\right)\right). \tag{A.2.7}$$

Fe(III) ions participate in hydrolysis reactions given by [11, 17]

$$\text{Fe}^{+3} + \text{H}_2\text{O} \overset{K_1}{\leftrightarrow} \text{Fe(OH)}^{+2} + \text{H}^+$$

$$\text{Fe}^{+3} + 2\text{H}_2\text{O} \overset{K_2}{\leftrightarrow} \text{Fe(OH)}_2^+ + 2\text{H}^+$$

$$\text{Fe}^{+3} + 3\text{H}_2\text{O} \overset{K_3}{\leftrightarrow} \text{Fe(OH)}_3 + 3\text{H}^+$$

$$\text{Fe}^{+3} + 4\text{H}_2\text{O} \overset{K_4}{\leftrightarrow} \text{Fe(OH)}_4^- + 4\text{H}^+$$

$$\text{Fe(OH)}^{+2} + \text{H}_2\text{O} \overset{K_5}{\leftrightarrow} \text{Fe(OH)}_2^+ + \text{H}^+$$

$$2\text{Fe}^{+3} + 2\text{H}_2\text{O} \overset{K_6}{\leftrightarrow} \text{Fe}_2\text{(OH)}_2^{+4} + 2\text{H}^+.$$

The hydrolysis constants are defined as follows:

$$K_1 = \frac{a^{\text{Fe}^{+3}}}{a^{\text{Fe(OH)}^{+2}} a^{\text{H}^+}},\ K_2 = \frac{a^{\text{Fe}^{+3}}}{a^{\text{Fe(OH)}_2^+} \left(a^{\text{H}^+}\right)^2},$$
$$K_5 = \frac{a^{\text{Fe(OH)}^{+2}}}{a^{\text{Fe(OH)}_2^+} a^{\text{H}^+}} \tag{A.2.8}$$

$$K_3 = \frac{a^{\text{Fe}^{+3}}}{a^{\text{Fe(OH)}_3} \left(a^{\text{H}^+}\right)^3},\ K_4 = \frac{a^{\text{Fe}^{+3}}}{a^{\text{Fe(OH)}_4^-} \left(a^{\text{H}^+}\right)^4} \tag{A.2.9}$$

$$K_6 = \frac{\left(a^{\text{Fe}^{+3}}\right)^2}{a^{\text{Fe}_2\text{(OH)}_2^{+4}} \left(a^{\text{H}^+}\right)^2}. \tag{A.2.10}$$

Activity of Fe^{+3} ions can be expressed as follows:

$$a^{\text{Fe}^{+3}} = a^{\text{Fe(OH)}_4^-} K_4 \left(a^{\text{H}^+}\right)^4. \tag{A.2.11}$$

Taking into account (6), (A.2.11), and (A.2.7), Butler–Volmer equation for the overall cathode electrochemical reaction can be written as

$$I^{\text{Fe}} = I_0^{\text{Fe}} \left(\frac{c^{\text{Fe(OH)}_4^-}}{c_{\text{ref}}^{\text{Fe(OH)}_4^-}}\right)^2 \frac{c^{\text{OH}^-}}{c_{\text{ref}}^{\text{OH}^-}} \left(\exp\left(\frac{\alpha_{\text{A}}^{\text{C}} F}{\text{RT}}\left(\eta^{\text{C}} - \eta_{\text{eq}}^{\text{C}}\right)\right) - \exp\left(-\frac{\alpha_{\text{C}}^{\text{C}} F}{\text{RT}}\left(\eta^{\text{C}} - \eta_{\text{eq}}^{\text{C}}\right)\right)\right) \tag{A.2.12}$$

where I_0^{C} is the cathode exchange current density; $c_{\text{ref}}^{\text{Fe(OH)}_4^-}$ is the reference concentration of Fe(OH)_4^- ions; and η^{C} is the potential difference at the cathode electrode/electrolyte interface.

Hydrogen dissolved in liquid phase is in equilibrium with hydrogen ions at the cathode electrode surface. The equilibrium concentration of hydrogen ions is calculated using Nernst equation defined for equilibrium electrochemical reaction of hydrogen oxidation

$$c_{\text{eq}}^{\text{H}^+} = 1000\, a^{\text{H}^+} \Big/ \gamma^{\text{H}^+},\ E = \frac{\text{RT}}{F} \ln\left(\frac{a^{\text{H}^+}}{a_{\text{H}_2}^{0.5}}\right). \tag{A.2.13}$$

Gas content in equilibrium gas–liquid mixture can be calculated from equilibrium flash equation

$$\sum_{k=1}^{n} \frac{\left(K^{(k)} - 1\right) Z^{(k)}}{\left(K^{(k)} - 1\right)\left(1 - \gamma_{\text{G}}\right) + 1} = 0 \tag{A.2.14}$$

where γ_{G} is the local splitting factor; $K^{(k)}$ is the distribution of the each components between the vapor and liquid phases, $K^{(k)} = y^{(k)} \big/ x^{(k)}$; and $Z^{(k)}$ is the mixture concentration. The linkage between molar splitting factor and gas volume fraction is given by

$$\alpha_{\text{G}} = \frac{\gamma_{\text{G}} \rho_{\text{L,mol}}}{\gamma_{\text{G}} \rho_{\text{L,mol}} + \gamma_{\text{L}} \rho_{\text{G,mol}}}. \tag{A.2.15}$$

Interfacial area of solid particles in suspension is

$$a_{\text{v}} = \frac{6}{d_{\text{p}}} \varepsilon_{\text{d}}. \tag{A.2.16}$$

For suspended particles in liquid flow, mass transfer coefficient in liquid phase is calculated from an empirical correlation [30, 31]

$$\text{Sh} = C \cdot (\text{Sc} \cdot \text{Ar})^{1/3} \tag{A.2.17}$$

where C is the constant; Sh is the Sherwood number; Sc is the Schmidt number; and Ar is the Archimedes number. The total component balance is written for parallel-plate reactor as follows

$$M_{\text{deposition}}^{\text{Fe}} = M_{\text{transfer}}^{\text{Fe}} + M_{\text{dissolving}}^{\text{Fe}}. \tag{A.2.18}$$

Component flow due to the diffusion flow of $Fe(OH)_4^-$ ions at the cathode electrode is

$$M_{\text{transfer}}^{\text{Fe}} = \int_S \left(-D_{\text{Fe(OH)}_4^-} \nabla c^{\text{Fe(OH)}_4^-}\right) \mathrm{d}S. \quad \text{(A.2.19)}$$

Component flow due to the iron deposition at the cathode electrode is

$$M_{\text{deposition}}^{\text{Fe}} = \frac{v^{(\text{Fe})}}{n_e^{(\text{Fe})} F} \left| I_{\text{avg}}^{\text{C}} \right| \cdot S_{\text{cell}}. \quad \text{(A.2.20)}$$

The component flow due to dissolving solid particles in suspension electrolysis is

$$M_{\text{dissolving}}^{\text{Fe}} = \int_V \beta_{\text{f,L}} a_{\text{v}} \left(c_{\text{eq}}^{\text{Fe(OH)}_4^-} - c^{\text{Fe(OH)}_4^-}\right) \mathrm{d}V. \quad \text{(A.2.21)}$$

The main conclusion is that the partial dissolution of solid particles compensates the component flow of iron deposition at the cathode electrode

$$S_{\text{transfer}} + S_{\text{dissolving}} = 1, \quad \text{(A.2.22)}$$

where S_{transfer} is the contribution of diffusion process, $S_{\text{transfer}} = \left|M_{\text{transfer}}^{\text{Fe}}\right| \Big/ \left|M_{\text{deposition}}^{\text{Fe}}\right|$ and $S_{\text{dissolving}}$ is the contribution of the dissolution process in combined chemical and electrochemical processes, $S_{\text{dissolving}} = \left|M_{\text{dissolving}}^{\text{Fe}}\right| \Big/ \left|M_{\text{deposition}}^{\text{Fe}}\right|$.

References

1. Okada G, Guruswamy V, Bockris JM (1981) J Electrochem Soc 128:2097–2102
2. Fourcade F, Tzedakis T (2000) J Electroanal Chem 493:20–27
3. Paramguru RK, Küzeci E, Kammel R (1988) Metall Trans B 19:59–65
4. Allanore A, Lavelaine H, Birat JP, Valentin G, Lapicque F (2010) J Appl Electrochem 40:1957–1966
5. Allanore A, Lavelaine H, Valentin G, Birat JP, Lapicque F (2008) J Electrochem Soc 155:E125–E129
6. Allanore A, Lavelaine H, Valentin G, Birat JP, Lapicque F (2007) J Electrochem Soc 154:E187–E193
7. Wang CY, Gu WB, Liaw BY (1998) J Electrochem Soc 145:3407–3417
8. Gu WB, Wang CY (2000) J Electrochem Soc 147:2910–2922
9. Newman J, Tiedemann W (1975) AIChE J 21:25–41
10. Haussener S, Xiang C, Spurgeon JM, Ardo S, Lewis NS, Weber AZ (2012) Energy Environ Sci 5:9922–9935
11. Stefánsson A (2007) Environ Sci Technol 41:6117–6123
12. Allanore A, Feng J, Lavelaine H, Ogle K (2010) J Electrochem Soc 157:E24–E30
13. Bockris JM, Huq AS (1956) Proc R Soc Lond A 237(1209):277–296
14. Balej J (1985) Int J Hydrogen Energy 10:365–374
15. Hurlen T (1960) Acta Chem Scand 14:1533–1554
16. Diakonov II, Schott J, Martin F, Harrichourry JC, Escalier J (1999) Geochim Cosmochim Acta 63:2247–2261
17. Blesa MA, Matijević E (1989) Adv Colloid Interface Sci 29:173–221
18. Cruz RCD, Reinshagen J, Oberacker R, Segadães AM, Hoffmann MJ (2005) J Colloid Interface Sci 286:579–588
19. Kastening B, Boinowitz T, Heins M (1997) J Appl Electrochem 27:147–152
20. Newman JS (1973) Electrochemical systems. Prentice-Hall Inc., Englewood Cliffs
21. Levin AI (1972) Theoretical fundamentals of electrochemistry. Metallurgiya, Moscow
22. Purday HFP (1949) An introduction to the mechanics of viscous flow; film lubrication, the flow of heat by conduction and heat transfer by convection. Dover Publications, Mineola
23. St-Pierre J, Piron DL (1986) J Appl Electrochem 16:447–456
24. Jupudi R, Zhang H, Zappi G, Bourgeois R (2009) J Comput Multiph Flows 1:341–348
25. Danilov VA, Tade MO (2009) Int J Hydrogen Energy 34:8998–9006
26. Bozbiyik B, Danilov VA, Denayer JF (2011) Int J Hydrogen Energy 36:14552–14561
27. Bansal R (2004) Handbook of engineering electromagnetics. Marcel Dekker, New York
28. Zemaitis JF, Clark DM, Rafal M, Scrivner NC (2010) Handbook of aqueous electrolyte thermodynamics: Theory & application. Wiley, New York
29. Bianchi H, Corti HR, Fernandez-Prini R (1994) J Solution Chem 23:1203–1212
30. Akselrud GA (1970) Mass exchange in the solid-liquid system (Soviet monograph on mass exchange in solid-liquid system covering soluble material extraction and absorption, interphase mass transfer and dissolving process)
31. Akselrud GA, Bojko AE, Kashcheev AE (1991) J Eng Phys Thermophys 61:98–102